Catalysis Today 143 (2009) 364–373

Contents lists available at ScienceDirect

Catalysis Today

journal homepage: www.elsevier.com/locate/cattod

Operando FTIR study of the photocatalytic oxidation of acetone in air over TiO_2–ZrO_2 thin films

María D. Hernández-Alonso [a], Isabel Tejedor-Tejedor [b], Juan M. Coronado [c,*], Marc A. Anderson [b], Javier Soria [a]

[a] *Instituto de Catálisis y Petroleoquímica, CSIC, c/Marie Curie, 2 Cantoblanco, 28049 Madrid, Spain*
[b] *Environmental Chemistry and Technology Program, University of Wisconsin, 660 North Park Street, Madison, WI 53706, USA*
[c] *Environmental Applications of Solar Energy, CIEMAT-PSA, Avenida Complutense 22, Bldg. 42, 28040 Madrid, Spain*

ARTICLE INFO

Article history:
Available online 3 April 2009

Keywords:
Photocatalysis
TiO_2
ZrO_2
In situ FTIR
Reaction mechanism
Thin films

ABSTRACT

Operando FTIR spectroscopy has been used to study the photocatalytic oxidation of acetone vapors over semiconductors films containing TiO_2 and ZrO_2. Preparation of these coatings was carried out by dipping a silicon wafer in stable sols containing particles of TiO_2, $Ti_{1-x}Zr_xO_2$, or a mixture of ZrO_2 and TiO_2. These differences in chemical composition and phase homogeneity were selected in order to determine their effect on the photocatalytic performance. A transmission cell specifically designed for *in situ* studies of photocatalytic coatings was utilized for the FTIR experiments under reaction conditions. In contrast with investigations with powdered photocatalysts, the use of thin films guarantees that the whole semiconductor is irradiated, and for that reason purely photochemical reactions are monitored. Acetone adsorption takes place molecularly and is higher on the $Ti_{1-x}Zr_xO_2$ coating. This fact is very likely related to the higher specific surface of the samples containing Zr. However, the maximum photocatalytic rate for acetone degradation corresponds to the films composed by a binary mixture of TiO_2 and ZrO_2. On the other hand, remarkable differences on the type and concentration of intermediates appearing as a result of the photocatalytic oxidation of acetone are found for the coatings studied. A simple kinetic model was applied to analyze the evolution of both gas phase and surface species. The parameters obtained indicate that each specific surface process is affected in a different way by the variation in the composition of the photoactive films.

1. Introduction

Heterogeneous photocatalysis with TiO_2 is becoming a well-established technology for pollution remediation. In this way, a growing number of devices and materials are commercially available in Japan and other countries [1,2]. Surprisingly, a detailed understanding of the mechanisms of photocatalytic processes is far from being complete, and several aspects, like the interpretation of the kinetic data, or the molecular details of self-cleaning surfaces, are still subject of an intense debate [3,4]. Nevertheless, in the last few years a significant deal of information has been gathered from molecular level studies of the degradation of different chemicals over irradiated TiO_2. *In situ* spectroscopic techniques like ESR [5,6], FTIR [7–13] and NMR [14,15] have been utilized to identify reaction intermediates, and to monitor the progress of the photocatalytic processes on the semiconductor surface. In particular, FTIR is a very powerful technique for mechanistic studies because it provides a high sensitivity and a relative rapid response, which allows the tracking of variations in the composition occurring in seconds. However, most of these studies have been carried out under idealized conditions in order to reduce interferences and facilitate the analysis of key chemical species generated during the reaction. Such simplification of the photocatalytic process may result in the loss of relevant information concerning reaction mechanisms. In fact, the possible distortions of the reaction pathways caused by unrealistic experimental parameters (i.e. reduced pressures, high concentration of reagents, etc.) is a general concern of catalytic studies, and consequently a rising number of the studies of catalytic reactions are performed under *operando* conditions [16]. This methodology employs the simultaneous analysis of the products of the reaction as well as the catalytic surface, and it can make possible a better understanding of the correlation between structure and activity of the catalysts. Interestingly, investigation of photocatalytic reactions has scarcely adopted an *operando* approach [7,11], very likely due to the difficulties of bringing together photocatalysts, reagents, light and

* Corresponding author. Tel.: +34 91 3466177; fax: +34 91 3466037.
E-mail address: juanmanuel.coronado@ciemat.es (J.M. Coronado).

0920-5861/$ – see front matter © 2009 Elsevier B.V. All rights reserved.
doi:10.1016/j.cattod.2009.02.033

analytical equipment. In fact, an efficient illumination of the portion of the photocatalysts sampled by the IR beam may be difficult, and consequently the possible contribution of chemical reactions in the dark areas of the solid could complicate the interpretation of the results. This problem can be circumvented by deposing the photocatalysts as thin film on ATR sampling devices [17], or an IR transparent substrate for spectra acquisition in the transmittance mode [18]. This last approach is very attractive for both, air purification systems and self-cleaning materials, because such applications require supported photocatalysts, which frequently are deposited as thin films.

Incorporation of heteroatoms in either cationic [19–21] or anionic [22] sites of the TiO_2 lattice, along with the formation of junctions with a second semiconductor [23,24], are among the most widely used strategies for improving the photoactivity of TiO_2. An interesting example of this approach is the synthesis of ZrO_2–TiO_2 photocatalysts with different compositions and phase distributions [24–27]. Although Zr does not modify significantly the optical properties of TiO_2, most of these studies report that by incorporating this element, one obtains superior photocatalytic performance. This has been related to the increment of either surface area, acidity or the density of active sites [24–27], but a more complete understanding of the photoactivity of these composite materials is required in order to take full advantage of their potential.

The aim of the present work is to determine the influence of the structural characteristics of ZrO_2–TiO_2 samples on the photodegradation of acetone at the molecular level. For this purpose, thin films of TiO_2, $Ti_{1-x}Zr_xO_2$ and ZrO_2/TiO_2 were deposited on Si wafers and their photocatalytic activity for the degradation of acetone vapors were investigated by transmission FTIR under *operando* conditions [16]. Acetone was chosen because it has widely been used as a model pollutant in other studies [8,11,12] and it is frequently detected in indoor air analysis [28]. The simultaneous analysis of surface and gas phase species allows one to measure kinetic parameters that can be used to ascertain the mechanism of acetone photodegradation, as well as to determine the structural and surface features which dictate the different performance of the studied samples.

2. Experimental

2.1. Preparation of the thin films

The TiO_2–ZrO_2 coatings used in this study were synthesized by sol–gel methods, as detailed described elsewhere [24,26], using $Ti(OPr^i)_4$ and $Zr(OPr^n)_4$ (Aldrich) as precursors. The sols were prepared by adding the corresponding alkoxides to water (ratio $M(OPr)_4/H_2O \approx 0.083$, v/v) acidified with nitric acid (ratio $HNO_3/H_2O \approx 0.020$, v/v for Zr-containing materials). In all cases, the corresponding oxide was initially precipitated. However, following 2 days of stirring complete peptisation was achieved, yielding homogeneous translucent sols. Subsequently, these acidic sols were dialyzed to a final pH in the range of 2.8–3.1. A mixed oxide having a nominal composition $Ti_{0.90}Zr_{0.10}O_2$ (labelled SS) was synthesized from the simultaneous hydrolysis of both metal alkoxides first in n-propanol solution and subsequently in excess water, while TiO_2 was obtained by direct hydrolysis of the alkoxide in water. On the other hand, $10\%ZrO_2/TiO_2$ coupled metal oxides (denoted Z/T) were obtained using TiO_2 and ZrO_2 sols prepared separately before blending them in the adequate proportions. Silicon wafers discs (Silicon Quest International) having 5 cm in diameter and about 615 μm in thickness were used as substrate. Three layers of the photocatalyst were deposited onto the washed substrate using a dip-coating technique at a withdrawal rate of 4 mm/s. An adequate wetting of the Si wafer was attained by adding to the sols a small amount of a perfluorinated surfactant (FC-4430, 3 M). After applying each layer, the discs were dried in air at 100 °C for 1 h and following the deposition of the third layer, the samples were fired at 350 °C for 2 h at a heating rate of 10 °C min^{-1}. Xerogels obtained from the same sols were used to estimate some of the structural properties of these thin films.

2.2. Physicochemical characterization

The pore size distribution and specific surface area of xerogels fired at 350 °C were determined from the N_2 isotherm analysis at 77 K in a Micromeritics ASAP 2010 analyzer. XRD patterns of ground xerogels were recorded on a Seifert XRD 3000P diffractometer using nickel-filtered Cu K_α radiation. The thickness of each photoactive layer was measured in Gaertner ellipsometer using light of $\lambda = 632.8$ nm and an incident angle of 70°. The refraction index and the thickness were calculated with the software provided by Gaertner Scientific Corporation.

2.3. Photocatalytic reactor for operando studies

A schematic representation of the system used for the simultaneous analysis of surface and gas composition during photocatalytic reactions is displayed in Fig. 1. The experimental setup consisted of a gas line loop which goes through the sampling space of two coupled FTIR spectrometers (Nicolet Nexus 670 and Magna 750 Series II, Madison, WI) both provided with MCT-A detectors cooled by liquid N_2. One of these spectrometers was equipped with a 4.8-m permanently aligned FTIR multiple-reflection gas sample cell (Model 4.8-PA, Infrared Analysis Inc., Anaheim, CA), while the other is endowed with a home-made transmission cell, which contains the Si wafer coated with the photocatalyst. Gas analysis was carried out by accumulating 64 scans at 1 cm^{-1} of resolution, while the transmission spectra of the photocatalytic layer were recorded after 200 scans at 4 cm^{-1} of resolution. The internal configuration of the cell for the photocatalytic thin films can be appreciated in the cross-section view shown in Fig. 2. The design is akin to that used in previous studies

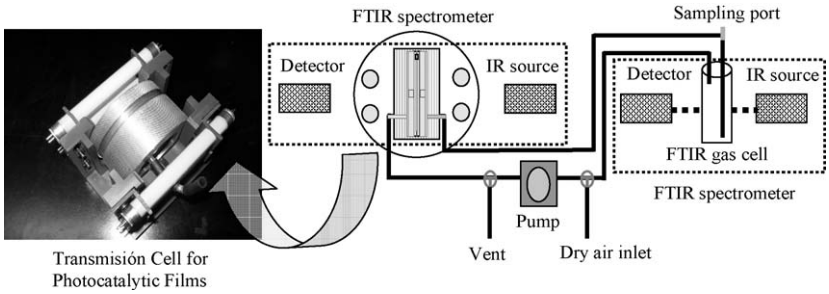

Fig. 1. Scheme of the setup for FTIR *operando* studies of photocatalytic reactions, which comprises the gas line loop and the two spectrometers for the analysis of gas and solid surfaces, respectively. The photograph shows a view of the transmission cell designed for the study of thin films of photocatalysts. After dosing the pollutant, this system operates as a recirculation photo-reactor as the gas flow is impelled by the pump. The vent and the dry air inlet are used to flush the system once the assay is finished.

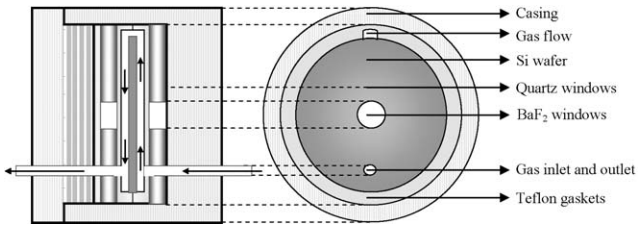

Fig. 2. Cross-section view of the cell used to test the photocatalytic activity of the thin films showing the path followed by the gas stream inside this device and the materials used for manufacturing the different components.

[18], although some modifications are introduced in order to maximize the contact between the photocatalysts and the gas phase. In particular the gas stream was forced to flow on the two sides of the wafer, following the path depicted with arrows in Fig. 2, which allows to increase the contact time. The casing of the cell was constructed of two threaded aluminium pieces with Teflon® gaskets and spacers to drive the gas streams into the required directions. Quartz windows ensure a good illumination of the coated wafer due to their transparency in the UVA range, while BaF_2 windows (9.5 mm of internal diameter, Harrick) allow FTIR sampling and they are moisture resistant. This cell acts as a photocatalytic reactor when it is irradiated with the four UV lamps (F4T5BL, 4 W, Black light, WIKO, Bulb Direct Co.), which are externally placed in an aluminium frame, as it is shown in Fig. 1. It is important to note that although the use of a second FTIR spectrometer can be necessary to detect gas phase intermediates formed at very low concentration (in the ppb range), information about the variations in the concentration of main products could be obtained with sufficient accuracy in a single FTIR instrument providing that interferences with the bands of the solid are not significant and, if the cell for "*in situ*" studies is designed with a longer optical path. On the other hand, some reference Attenuated Total Reflection (ATR) experiments were carried out using a single bounce Avatar® cell provided with a ZnSe optical element.

The photoreaction system for *operando* studies is provided with a pump having an internal ceramic body (Model Qd, Fluid Metering Inc.) that deliver the gas at a flow rate of 75 $cm^3\ min^{-1}$. An injection port with a septum for acetone dosing with a microsyringe (Aldrich, HPLC grade) and two three-way valves to allow recirculation of the gas during photocatalytic experiments, or flushing with air free of CO_2 and moisture for cleaning, complete the system. The total volume of the system was about 0.55 L.

3. Results

3.1. Characterization of the photocatalytic films

ZrO_2–TiO_2 materials prepared by the same sol–gel procedure have been extensively characterized in a previous work [26]. Table 1 summarizes the main structural and morphological properties of the samples used in the present study. These data were estimated either from analysing the corresponding xerogels, or directly from the film by ellipsometry. XRD analysis indicates that all the samples contained nanocrystalline anatase with a small proportion of brookite. These results have been independently confirmed by Raman scattering of the coatings [26]. In the case of sample SS, Zr incorporation seems to expand slightly the volume of the anatase unit cell (see Table 1), as can be expected for the partial substitution of Ti^{4+} by Zr^{4+}, which presents a larger ionic radius [25–27]. In contrast, the sample Z/T shows a minor increment of the cell volume, which reveals a lower degree of Zr insertion into the anatase phase.

In accordance with previous reports, Zr incorporation leads to a considerable increment of surface area with regards to unmodified TiO_2 [24,26]. On the other hand, both Zr-containing photocatalysts show comparable surface area, although the mean pore size is slightly narrower for sample Z/T. The thickness of the coatings varies from 410 to 540 nm due to differences in the number of layers and the viscosity of the sols employed to produce the coatings. Similarly, porosity roughly estimated from the refractive index measurements, and taking as reference the optical properties of bulk TiO_2–ZrO_2 materials [29,30], is higher than 44% for all the films, as is shown in Table 1.

3.2. Acetone adsorption

Fig. 3 displays the FTIR spectra of the photoactive coatings flushed with dry air for 5 min, and subsequently exposed to 12.2 $\mu mol\ L^{-1}$ of acetone for 40 min. The spectra of the solid films before adsorption, as well as the gas phase contribution, have been subtracted in order to highlight the features of adsorbed species. The spectra of the three studied samples are overall, rather similar although the intensity of the bands varies broadly for each material. The positions and assignments of the bands are listed in Table 2 [11,12]. According to the literature, most of these bands can be assigned to different vibration modes of acetone molecularly adsorbed on the photocatalytic coatings. In fact, these spectra resemble closely those measured by ATR for acetone–water mixtures (see Fig. 4Af), as discussed below. On the other hand, the negative band at 1639 cm^{-1} is due to the displacement of weakly adsorbed water molecules, while the sharper negative bands in the 3692–3635 cm^{-1} range can be attributed to the perturbation of the vibration of surface hydroxyls which interact with acetone molecules. Differences between samples in this spectral region reveal slightly dissimilar surfaces. This can be related to modifications of the morphology of the nanocrystals (i.e. crystallographic faces exposed) [31] and/or to the formation of distinct hydroxyls induced by Zr incorporation [27]. Such interactions between acetone and hydroxyls are as well responsible for the very broad and positive bands appearing between

Table 1
Textural and structural characteristics of the photocatalysts.

Sample	Cell volume[a] (Å^3)	Crystallite size[b] (nm)	S_{BET}[c] ($m^2\ g^{-1}$)	Mean pore size[c] (nm)	Film thickness[d] (nm)	Refractive index[d]	Porosity[e] (%)	Film mass ($\mu g\ cm^{-2}$)[f]
TiO_2	136.0	6.5	172	5.4	470	1.82	47	97
$Ti_{0.90}Zr_{0.10}O_2$–SS	137.1	6.4	269	5.3	540[g]	1.79	47	111
10%ZrO_2/TiO_2–Z/T	136.4	4.3	249	4.0	410	1.84	44	89

[a] Calculated from a least square fit of the XRD data of the corresponding xerogels.
[b] Calculated from XRD data of the xerogels using the Scherrer equation.
[c] Obtained from the N_2 adsorption isotherm of the xerogels.
[d] Measured in the thin films by ellipsometry.
[e] Estimated from the ellipsometric data.
[f] Calculated from anatase density, and the thickness and porosity of the films.
[g] Corresponding to six layers.

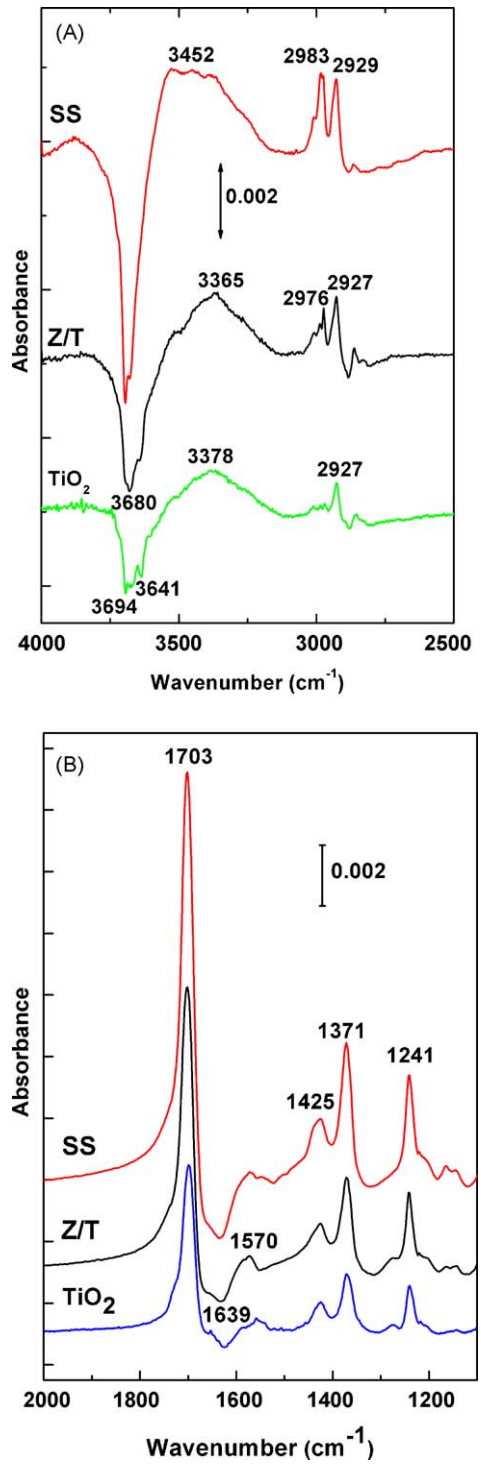

Fig. 3. FTIR spectra in the (A) 4000–2500 cm^{-1} and (B) 2000–1100 cm^{-1} range of the samples SS, Z/T and TiO_2 following exposure to acetone vapor (0.5 μL) and equilibrated for 40 min in the recirculation loop. Spectra of the solid before adsorption have been subtracted in order to highlight the bands corresponding to surface species.

3460 and 3360 cm^{-1}. Similar features have been also observed after adsorption of other organic molecules on TiO_2, and they have been attributed to the modification of the hydrogen bonding of the hydroxylated surfaces of the solid by the adsorbate [7–9,11,13].

The intensity of adsorbed acetone bands increases with increasing surface area, and it reaches a maximum for sample SS. Considering the thickness of the films and the surface area of the samples, it can be concluded that while TiO_2 and Z/T basically adsorb the same amount of acetone on a surface area basis, sample SS adsorbs about 1.7 times more acetone per surface area unit than pure TiO_2. Fig. 4A displays the variation of the spectra of sample Z/T with increasing acetone concentration, compared to the ATR spectra of an acetone–water mixture (ca. 40/60, v/v). Although a gradual shift of the bands is observed with increasing vapor pressure, the bands of adsorbed acetone are nearly coincident to that of the solution. These slight modifications of the spectra can be explained as a consequence of the increment of the interaction between acetone molecules in the adsorbed layer, in such a way that the spectra progressively approach that of neat liquid acetone. Such observations are in accordance with previous studies that indicate that acetone molecules do not experience any transformation after adsorption on hydrated TiO_2 surfaces [8,11,12]. Nevertheless, as mentioned above, the negative band at 1639 cm^{-1} reveals that acetone displaces water molecules weakly bonded to the oxide surface. Therefore, it is proposed that acetone molecules are attached to the solid surface by interacting the C=O group with hydroxyl groups, rather than by coordination to unsaturated surface cations, as it has been previously suggested [8]. Fig. 4B shows the corresponding adsorption isotherm of acetone on Z/T, with the equilibrium pressure obtained from the FTIR analysis of the gas phase and the adsorbed amount estimated from spectra of Fig. 4A taking the intensity of the band at about 1700 cm^{-1} (integrated between 1730 and 1660 cm^{-1}). Although the actual amount of adsorbed acetone cannot be quantified because the response factor of the surface species is unknown, it can be assumed that approaches to the monolayer at high acetone concentration. Thus, the variation of the coverage can be approximately reproduced using the Langmuir adsorption equation:

$$\theta_A = \frac{KP_A}{1 + KP_A} \quad (1)$$

where θ_A represents the acetone coverage, K the adsorption constant and P_A the acetone partial pressure. From the least square fitting of the data to the Langmuir expression a value of $K = 3.7 \times 10^6$ L mol^{-1} is obtained for Z/T. Adsorption results are qualitatively similar to those obtained by El-Maazawi et al. using TiO_2 Degussa P25 [12]. However, in contrast with previous studies with TiO_2 coatings on glass [11], multilayer adsorption does not seem to be significant under the conditions employed in the present study.

Table 2
Assignment of the bands of adsorbed acetone and the surface intermediate species formed during its photocatalytic degradation.

Surface species	Vibration mode	Frequency (cm^{-1})	
		Observed[a]	Literature[b]
Acetone	ν (C–H)	2975–80, 2927–29	2973, 2931
	ν (C=O)	1701–1685	1702–1689
	δ_{as} (CH_3)	1425–23	1422
	δ_s (CH_3)	1370–68	1366
	ν (C–C)	1241–35	1240
Formate	ν (CH)	2870	2877
	ν_{as} (COO)	1571	1575
	ν_s (COO)	1358	1358
Acetate	ν_{as} (COO)	1584	1582
	ν_s (COO)	1420	1415
Formaldehyde	ν (C=O)	1744–42	1746
Bicarbonate	ν_{as} (COO)	1447	1444

[a] Frequencies vary in the intervals given as a function of coverage.
[b] Refs. [8,9,11,12,32].

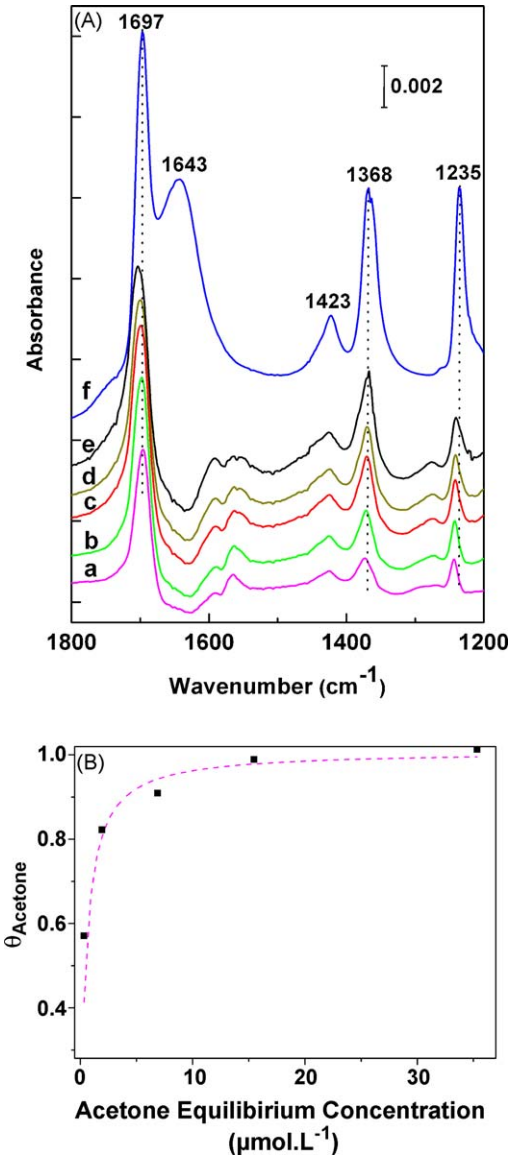

Fig. 4. (A) FTIR spectra of the sample Z/T exposed to increasing pressure of acetone vapor (a–e) along with (f) the ATR spectrum of a water–acetone mixture and (B) acetone adsorption isotherm which plots the coverage of acetone, θ, estimated from the intensity of spectra as a function of the equilibrium concentration obtained from FTIR analysis of the gas phase. The dashed line represents the least square fit of the data to the Langmuir equation, as explained in the text.

3.3. Operando study of the photocatalytic oxidation of acetone: surface analysis by FTIR

Upon UV illumination in air, the spectra of the films previously equilibrated with acetone are remarkably modified. These transformations can be observed in Fig. 5, which shows the evolution of the spectra of the different coatings with irradiation time. In the case of sample SS (see Fig. 5A and B) acetone bands decrease progressively after turning on the lamp, while new features at about 2870, 1742, 1571 (broad), 1452 and 1358 cm^{-1} develop. Significant overlapping of the peaks complicates precise identification of the intermediate species but, on the basis of previous studies, bands generated upon illumination can be related to distinct vibrational modes of formate, bicarbonate, and formaldehyde species adsorbed on the surface of the photocatalysts [7,9,11–13]. Theses bands and their assignments are summarized in Table 2. Initially the spectra are dominated by the band at 1571 cm^{-1} associated to the ν_{as} (COO) mode of formates, which are similar to those detected in previous studies in TiO_2 powders [9,11,12]. The intensity of this band grows progressively and reaches a maximum at about 40 min of irradiation. Few minutes before, the presence of formaldehyde becomes evident as the band at 1742 cm^{-1}, which corresponds to the ν (C═O) mode, starts to grow [12,32]. Following irradiation for more than 180 min, the overall intensity of the spectra of SS sample decreases significantly and the bands of acetone disappear almost completely. At this stage the proportion of formates drops with respect to formaldehyde, as indicated by the ratio between the corresponding bands. Further irradiation of the SS sample levels off the spectra (not shown). These results indicate that adsorbed species are fully removed at this stage. Consequently the initial state of the fresh photocatalytic surface can be recovered following prolonged irradiation, since even adsorbed water can be replenished with the molecules generated during the oxidation of acetone. In these regards, spectra of the sample SS in the 4000–2500 cm^{-1} range (Fig. 5A) show that, although during the initial stages of the reaction hydroxyl groups appear as relatively sharp negative bands at 3691 and 3674 cm^{-1} (see Fig. 5A), these signals progressively disappear as organic molecules are removed from the photoactive surface. In addition, the slight increment of the intensity at 3550 cm^{-1} observed after 180 min of irradiation suggests the adsorption of a small excess of water. In the case of sample Z/T, the spectra obtained (see Fig. 5C) are rather similar to those of SS, apart from minor variations in the frequencies of the bands. However, after 120 min of irradiation, formates have been almost completely removed, and the spectra of the SS coating show bands at 1744, 1540 and 1447 cm^{-1}. This last band can be assigned to the ν_{as} (COO) mode of bicarbonate, while the band at 1540 cm^{-1} very likely has contributions of the residual formates and the ν_s (COO) mode of bicarbonate [9,12]. On the other hand, the band at 1744 cm^{-1} can be attributed to the formation of formaldehyde, as in the case of Z/T [8,11,32]. In contrast, for TiO_2 coatings, the build-up of adsorbed intermediates is remarkably lower (see Fig. 5D), and the indication of the presence of formates is observed. The most intense bands following prolonged irradiation appears at 1371 and 1752 cm^{-1}. This last vibration is tentatively assigned to the C═O stretching mode of adsorbed aldehyde molecules. However, as this band is significantly blue-shifted with respect to those attributed to formaldehyde, it may correspond to other carbonyl species like formic acid [11].

Variation of the integrated intensity of adsorbed acetone (integrated between 1720 and 1660 cm^{-1}), along with the changes in the background intensity at 1020 cm^{-1} (integrated between 1000 and 1060 cm^{-1}) are shown in Fig. 6. In addition, the evolution of the intensity of formate (integrated between 1635 and 1500 cm^{-1}) is plotted for samples Z/T and SS, while the changes in aldehyde concentration (integrated between 1790 and 1730 cm^{-1}) is represented for TiO_2. Furthermore, this graph plots the evolution of CO_2 to facilitate comparison with gas phase data. Both photoactive coatings show comparable trends, which define three different stages (marked in Fig. 6 by dotted vertical lines) according to the coverage of intermediate species. In the first and shortest period, a rapid decrease of the amount of adsorbed acetone takes place in parallel to the rise of a formate species for the Zr-containing samples. In the case of TiO_2, this stage is characterized by a sharp increment of the band at 1750 cm^{-1}, while the acetone concentration remains basically constant. In the case of samples SS and Z/T, during the second stage the coverage of these adsorbed species can be considered roughly constant, although the concentration of formate slightly increases and acetone coverage progressively decays. In the case of TiO_2, although the amount of aldehyde remains basically constant in this period, the concentration of adsorbed acetone progressively decreases. Finally, in the last period the concentration of all adsorbed species began to decrease, while CO_2 concentration reaches its maximum value. These tendencies are comparable with those observed over TiO_2 and Nb-doped films [8], although differing from

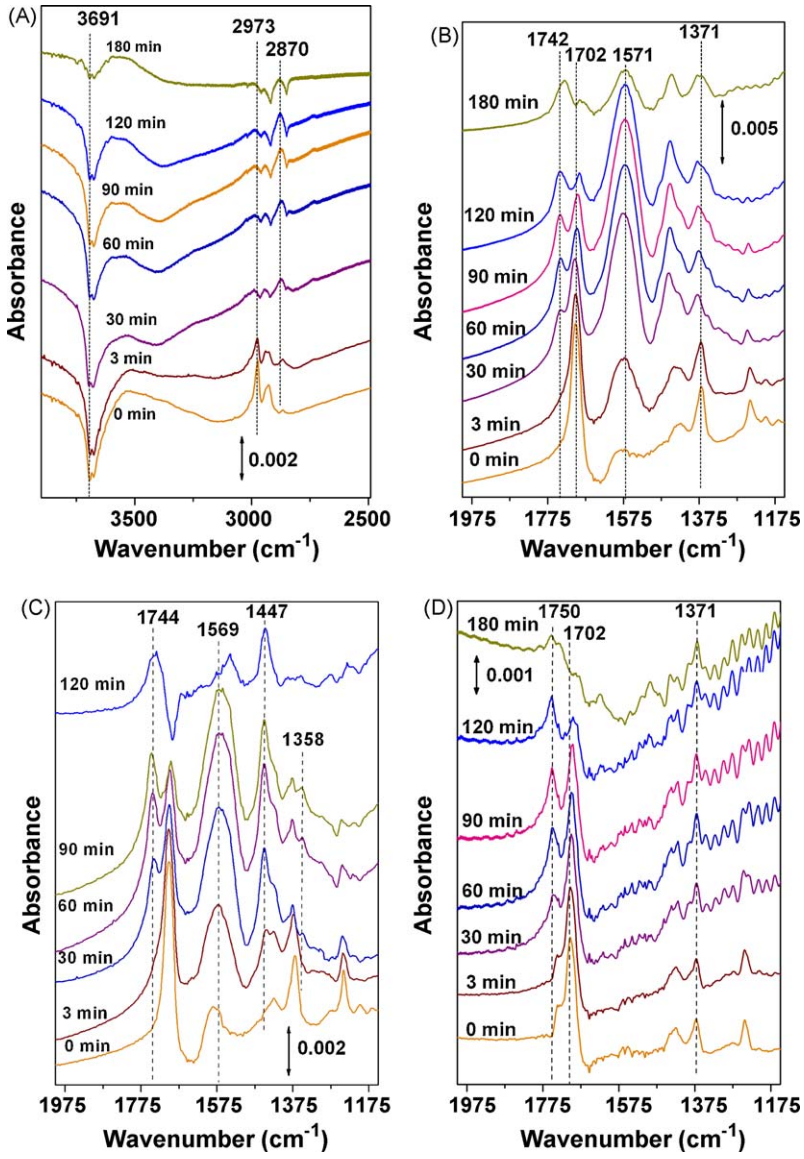

Fig. 5. FTIR spectra in the (A) 4000–2500 cm^{-1} and (B–D) 2000–1150 cm^{-1} range of the sample (A and B) SS, (C) Z/T and (D) TiO_2 contacted with acetone vapor (0.5 μL of liquid) and subsequently UV-irradiated for increasing periods of time as indicated in graphs. Spectra of the photocatalytic coating before acetone adsorption have been subtracted in order to highlight the bands corresponding to surface species.

the results obtained with TiO_2 powders, which does not show the removal of adsorbed intermediates [11,12]. These differences are very likely due to the inefficient illumination of thicker layers of photocatalyst, which causes the accumulation of intermediates in shaded areas.

Photogenerated conduction band electrons can be detected upon UV irradiation of TiO_2 by FTIR because they cause an increment in the otherwise featureless spectral intensity, which is more marked at lower wavenumber [4,33]. As shown in Fig. 6, this effect is also clearly detected during photocatalytic degradation of acetone in the studied coatings. Here the increment in background intensity at ca. 1020 cm^{-1} as a function of irradiation time has been plotted. The shape of these curves is similar to those obtained with TiO_2 powder in vacuum at sub-ambient temperatures [33], although the period for reaching a steady intensity is considerably longer in the present case. This difference is very likely related to the presence of molecular oxygen, which being an electron acceptor, should contribute to reduce the density of photogenerated electrons. Uncoated silicon wafers also show this behaviour due to their semiconductor character. In fact, silicon wafer presents the highest intensity of the IR background signal (not shown). Among coated samples the highest electronic density is achieved by TiO_2 followed by SS and finally Z/T samples. On the other hand, it is also worth noting that the accumulation of free electrons can be also detected by the increment of the interference fringes of the films, which also gain amplitude as it can be appreciated in Fig. 5D. Although these fringes are almost undetectable for the coatings studied, they can be very intense when using thinner Si wafers as substrates. This observation suggests that the refractive index of these coatings increases under UV-irradiation due to the formation of photogenerated electrons, and therefore these coatings behave as photorefractive materials, in a similar way to other metal oxide thin films deposited on Si [34].

3.4. Operando study of the photocatalytic oxidation of acetone: evolution of gas phase composition

Results of the photocatalytic degradation of acetone over the different coatings are displayed in Fig. 7, as obtained by gas phase analysis. This graph represents the variation of the fractional

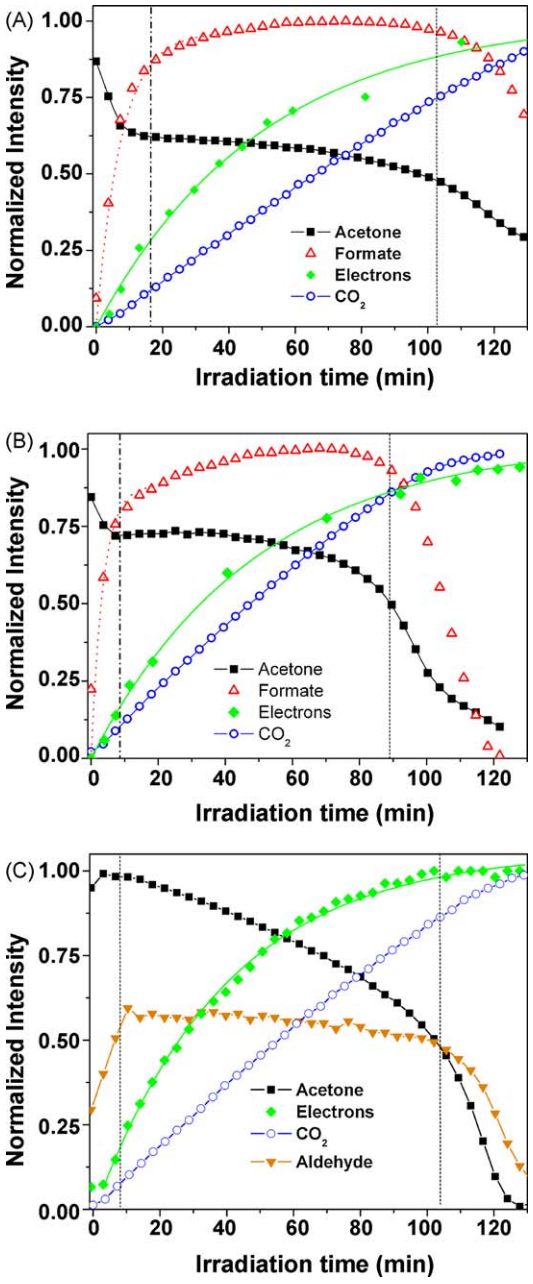

Fig. 6. Variation of the normalized intensities of adsorbed acetone (squares) and formate (up-triangles) and aldehydes (down-triangles) detected during UV-irradiation of the (A) SS, (B) Z/T and (C) TiO_2 samples. Evolution of CO_2 production (circles) along with the relative concentration of photogenerated electrons (diamonds) is also plotted for comparison. Vertical lines mark the different stages of the photocatalytic processes. The proposed kinetic model (see main text for a detailed discussion) has been used in (A) and (B) to establish the end of the initial period (vertical dotted and dashed line) and to model the variation of formate coverage (dotted line). The remaining lines are solid lines are only visual guides.

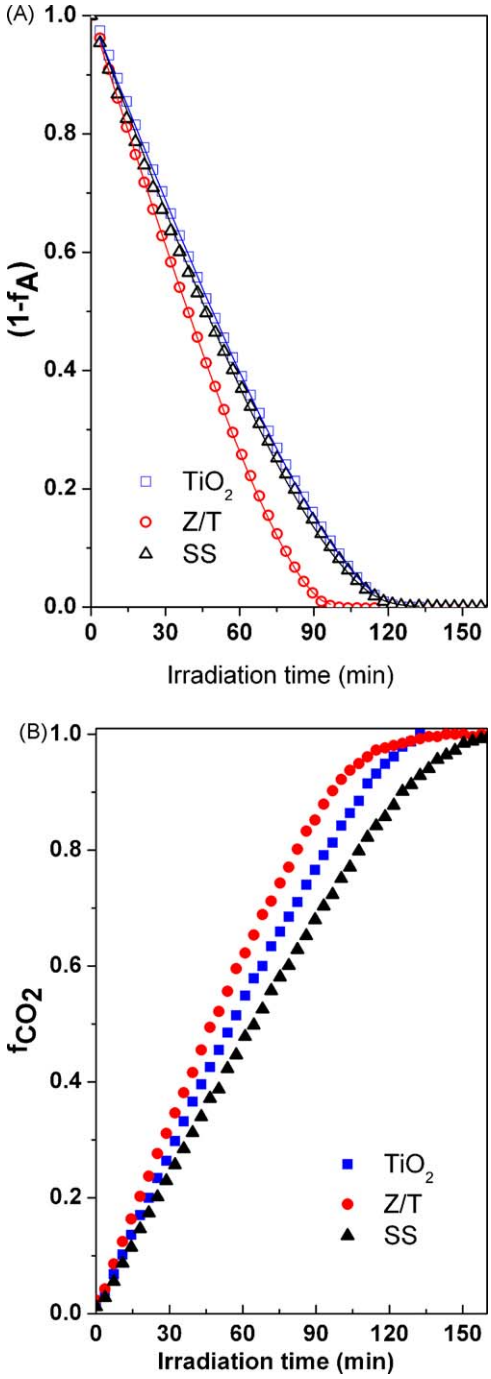

Fig. 7. (A) Variation of the fractional conversions of acetone vapor, f_A, and (B) CO_2 production, f_{CO_2}, with irradiation time in the presence of TiO_2 (square), Z/T (circle) or SS (triangle) photocatalytic coatings. The solid lines plotted in (A) represents the least square fit of the data to the Langmuir–Hinshelwood model, as explained in the text.

conversions of acetone (Fig. 7A) and CO_2 (Fig. 7B), defined as

$$f_A = \frac{1 - C_{A(g)}}{C^0_{A(g)}} \quad (2)$$

$$f_{CO_2} = \frac{C_{CO_{2(g)}}}{3C^0_{A(g)}} \quad (3)$$

where $C^0_{A(g)}$ and $C_{A(g)}$ are acetone concentration, just before turning on the UV-lamps and after a certain period of irradiation, respectively, while $C_{CO_{2(g)}}$ refers to CO_2 concentration. In accordance with previous studies [8,11,12], no products apart from CO_2, H_2O and minor amounts of CO were detected in the gas phase. These data clearly indicate that the oxidation rate is significantly larger for sample Z/T, while TiO_2 and SS show almost coincident rates, although the plot of CO_2 production (see Fig. 7B) clearly shows that the sample SS presents a lower rate. Furthermore, if differences in mass are estimated from the thickness and porosity of the films, the normalized rate for the SS coating becomes the lowest, as indicated in Table 3. On the other hand, it is worth noting

Table 3
Kinetic parameter obtained from the models for the evolution of surface and gas phase species as described in the text.

Sample	Initial rate			Surface species		Gas phase (LH)	
	r_{Acet} (mol s^{-1} m^{-2})[a]	r_{Acet} (mol s^{-1} g^{-1})[b]	r_{CO_2} (mol s^{-1} g^{-1})[b]	k_1 (s^{-1})	k_2 (s^{-1})	K' (L mol^{-1})	k' (mol s^{-1})
TiO_2	1.77×10^{-9}	3.045×10^{-7}	2.704×10^{-7}	–	–	780,269	1.30×10^{-9}
SS	1.07×10^{-9}	2.891×10^{-7}	1.999×10^{-7}	1.08×10^{-3}	8.20×10^{-5}	725,887	1.38×10^{-9}
Z/T	1.65×10^{-9}	4.115×10^{-7}	3.437×10^{-7}	2.05×10^{-3}	5.43×10^{-4}	955,886	1.60×10^{-9}

[a] Normalized by the surface area.
[b] Normalized by mass of photoactive coating.

that, for all the samples, the CO_2 production rate is slightly lower than that of acetone removal (see Table 3). In the absence of any volatile intermediates, this observation indicates that partial oxidation products are building up in the photoactive layers, in agreement with the simultaneous FTIR analysis of the films surface. This is particularly evident in the case of the SS coating, which shows a significant difference between the acetone degradation and the CO_2 production rates.

4. Discussion

4.1. Mechanism of acetone photocatalytic oxidation

Surface science investigations using single-crystal rutile (1 1 0) reveal that acetone degradation proceeds with the formation of surface acetate and the simultaneous release of methyl radicals in a two-step process [35]. On the other hand, based on the ESR analysis of acetone photocatalytic degradation on polycrystalline TiO_2, Attwood et al. [6] proposed that the reaction initiates by the surface trapped holes, O^-, according to the following processes:

$$CH_3COCH_3 + O^- \rightarrow CH_3COCH_2^\bullet + OH^- \quad (4)$$

$$CH_3COCH_2^\bullet + O_2 \rightarrow CH_3COCH_2OO^\bullet \quad (5)$$

These peroxyl radicals are rather unstable and they decompose easily. This process can take place according to several routes but eventually they drive the breakage of a C–C bond. In this respect, a plausible reaction pathway is the following:

$$CH_3COCH_2OO^\bullet + O^- \rightarrow CH_3CHO + CO_2 + OH^- \quad (6)$$

that very likely implies several elementary steps of molecular rearrangement. The formation of adsorbed acetaldehyde on the TiO_2–ZrO_2 coatings during photocatalytic oxidation of acetone has not been confirmed because the corresponding C=O stretching band at 1718 cm^{-1} could be masked by the vibrations of other species. In any case, considering that in accordance with previous reports [8,10–12], only CO_2, H_2O and a small amount of CO are detected in the gas phase, it can be concluded that acetaldehyde transformation occurs at a higher rate that its desorption. Photocatalytic oxidation of acetaldehyde could yield acetic acid that remains adsorbed on the surface as the acetate complexes detected by FTIR in previous reports [8,10–12]. Further oxidation of these species could yield formate, which is clearly detected in the case of the Zr-containing coatings, and eventually CO_2. In addition, formation of formaldehyde from acetaldehyde has been also judged possible [36,37]. Results obtained in the present work are consistent with these two simultaneous degradation routes, which can be schematically depicted as follows:

$$CH_3CHO \rightarrow CH_3COO^- + H^+ \rightarrow HCOO^- + H^+ \rightarrow CO_2 \quad (7)$$

$$CH_3CHO \rightarrow HCHO \rightarrow HCOO^- + H^+ \rightarrow CO_2 \quad (8)$$

The existence of these parallel routes is consistent with the observation of aldehydes, very likely formaldehyde, following the complete removal of formates for ZrO_2–TiO_2 coatings (see Fig. 5A–C) [38]. This experimental fact most likely implies that the route (7) is faster, leading to the initial increment of formates. In contrast, degradation of acetaldehyde seems to take place according to reaction (8) for TiO_2 (see Fig. 5D). Formation of bicarbonate, which is particularly evident for sample Z/T, can be explained as a result of the interaction of either CO_2 or formate with the surface of these hydroxylated oxides [9]. On the other hand, the results obtained in the case of the TiO_2 film could be justified accepting that formaldehyde oxidation to formic acid is the rate limiting step in the (8) pathway. Finally, it is worth noting that, on the contrary to the results obtained with TiO_2 powders, an almost total regeneration of the film surface can be achieved. In contrast, in the case of the experiments performed with TiO_2 powders, intermediates can diffuse and accumulate in dark areas [10–12], when the semiconductor is deposited as a thin film the whole layer is activated and participates in the photocatalytic degradation process.

4.2. Kinetic aspects of acetone photocatalytic oxidation

Considering the remarkable differences in the evolution of the surface composition of the ZrO_2–TiO_2 samples, a kinetic analysis may provide further insight on the influence of these variations in photoactivity. However, due to the complexity of the acetone photo-oxidation mechanism, as it has been described in the previous section, a detailed model of this process can be unapproachable without complex calculations. Alternatively, the following simplified reaction scheme for the photocatalytic oxidation of acetone can be proposed in order to account for the key aspects of surface photoactivity:

$$CH_3COCH_3(g) \leftrightarrow CH_3COCH_3(ads) \xrightarrow[O_2]{k_1} 2HCOO^- + H^+ + CO_2 \xrightarrow[O_2]{k_2} 2CO_2 \quad (9)$$

This pathway contains three main steps, first acetone adsorption equilibrium, which is achieved rapidly, then the oxidation of adsorbed acetone to yield CO_2 and formate, which occurs with a kinetic constant of k_1, and, finally, the formate oxidation to CO_2, whose rate is defined by the kinetic constant, k_2. This brief scheme can justify the major features observed experimentally in Fig. 6A and B, and it allows an easy analysis of the data, considering the following approximations: (i) oxygen molecules are in excess and they do not compete for adsorption sites with organics, (ii) acetone and formate are adsorbed on the same centres, and (iii) oxidation of formaldehyde, which is also detected on the photocatalytic surface, is quicker than that of the formate [38], and consequently this process is not a rate-determining step. This last condition implies that the route described in Eq. (7) is the main one. This seems to be the case for the coating modified with Zr, but it is not true for TiO_2 which consequently cannot be analyzed by this model. In any case, the persistence of aldehyde bands following prolonged irradiation suggests that the last mineralization step surely includes additional stages which will not be considered in

this oversimplified model. Keeping in mind these assumptions, the initial stage upon UV-irradiation will imply the transformation of the adsorbed acetone to formate according to the following kinetic equation:

$$\frac{d\theta_A}{dt} = -k_1\theta_A \quad (10)$$

where θ_A stands for the acetone coverage. On the other hand, the variation of formate coverage, θ_F, is given by

$$\frac{d\theta_F}{dt} = 2k_1\theta_A - k_2\theta_F \quad (11)$$

Assuming that during this initial period the surface is saturated and consequently the concentration of vacancies is nil, then:

$$\theta_F + \theta_A = 1 \quad (12)$$

Substitution of the expression (12) in Eq. (11) leads to

$$\frac{d\theta_F}{dt} = 2k_1 - (2k_1 + k_2)\theta_F \quad (13)$$

Eq. (13), once integrated, yields the following expression for the variation of formate coverage:

$$\theta_F = a/b[1 - e^{-b}] \quad (14)$$

where $a = 2k_1$ and $b = (2k_1 + k_2)$. This equation was used to estimate k_1 and k_2 from the fitting of experimental data obtained just after irradiation (see dotted line in Fig. 6A and B), and the values of these parameters are collected in Table 3. These results indicate that the higher value of k_1 is obtained for Z/T, which is about double than in the case of SS. However, the most remarkable differences correspond to k_2, which is one order of magnitude lower for SS than for Z/T. From Eq. (14) it can be deduced that the coverage at the end of this stage should be proportional to $2k_1/(2k_1 + k_2)$, and accordingly the concentration of formate is about a 9% larger for SS than for Z/T. On the other hand, the time required to achieve the steady state coverage, τ_{st}, can be correlated to $1/(2k_1 + k_2)$, as it can be derived from Eq. (14). In this way the first vertical dashed line in Fig. 6A and B marks the time at which a 90% of the final coverage is reached.After this initial period of sharp decay, acetone coverage remains basically constant until the depletion of acetone vapor is almost complete. Similarly, the surface concentration of adsorbed intermediates does not vary significantly during this period (i.e. $d\theta_F/dt \approx 0$). Therefore, using the steady state approximation the following equivalences are obtained:

$$KP_A(1 - \theta_A - \theta_F) - \theta_A = 0 \quad (15)$$

$$2k_1\theta_A - k_2\theta_F = 0 \quad (16)$$

where K is the acetone adsorption constant, and P_A the acetone partial pressure. Combining these two equations yields:

$$\theta_A = \frac{KP_A}{(1 + K'P_A)} \quad (17)$$

where $K' = K(1 + 2k_1/k_2)$. This equation is equivalent to the expression (1) used for fitting the adsorption data. Finally, during the last period, the partial pressure of acetone approaches to zero, and both θ_A and θ_F start to decrease. In the case of TiO_2 films similar considerations could be made by assuming that in the steady state the rate of aldehyde formation equals that of the adsorbed acetone decomposition. However, for this sample after a short initial period, the acetone coverage decreases steadily first and steeply after about 100 min of irradiation. This fact indicates that a more direct correlation between acetone coverage and gas phase exits for this photocatalytic film. This fact can be related to the lower competition between acetone and intermediate species for adsorption sites.

Several studies have proposed the use of Langmuir–Hinshelwood model (hereafter denoted as LH) as a convenient kinetic description of the photocatalytic degradation of gas phase pollutants [39,40]. In the present case, as mentioned above, the study of surface species evolution indicates that, except for a short initial period, the steady state approximation can be applied to these processes. Therefore, considering that adsorption is a very rapid process, the degradation of adsorbed acetone is the rate determining step for gas phase removal of this molecule, and therefore Eqs. (10) and (17) can be combined to yield:

$$\frac{dP_A}{dt} = \frac{k'P_A}{(1 + K'P_A)} \quad (18)$$

where k' is the apparent kinetic constant. An equivalent equation can be obtained for TiO_2 just considering not-competitive acetone adsorption [40]. Gas phase data have been fitted using the integrated equation and the kinetic parameters obtained are collected in Table 3. As it is shown in Fig. 7A, this model reproduces perfectly the experimental data. As expected, the higher kinetic constant corresponds to the sample Z/T, while for the other samples differences are small, although this parameter is slightly higher for the doped catalyst, consistently with the slopes of the curves of Fig. 7A. Nevertheless, if both surface area and mass are considered, the specific activity of the sample SS becomes slightly lower than that of TiO_2. However, it is important noting that when the initial rates are normalized by the specific surface, the value for TiO_2 is slightly higher than for Z/T. On the other hand, adsorption constants can be ranked as follows: $Z/T \gg SS > TiO_2$. This parameter does not follow the same tendency found in the FTIR spectra. However, considering that K' is not only related to the adsorption capacity of the photocatalytic films, but it also participates of kinetic parameters, this ranking of the samples seems to be related alt least partly to the photoactivity of the films. Anyhow, discrepancies between the adsorption constant measured directly in the dark and obtained from kinetic data under illumination have been frequently reported [40,41]. In this particular case the adsorption constant in the dark, K, for Z/T is about four times larger than that K', as obtained from the kinetic model. Leaving apart the limitation of the model, this fact can be related to the rapid modification of the surface upon UV-irradiation, as revealed by FTIR spectra. Thus, the formation of surfaces complexes like formates modifies the interaction of acetone molecules with the surface and reduces the number of sites available for adsorption.

4.3. Influence of the chemical composition and phase distribution of ZrO_2–TiO_2 photocatalyst on photoactivity

Zirconium incorporation has been found to enhance the photoactivity of TiO_2 in samples prepared either by sol–gel methods [24] or microemulsions [27]. Furthermore, previous studies have shown that mixed oxides $Ti_{1-x}Zr_xO_2$ are more efficient for the photocatalytic degradation of airborne methylcyclohexane than binary ZrO_2/TiO_2 oxide [27]. However, in case of coatings on glass, it has been reported that zirconium is slightly detrimental for the photoactivity [26]. The origin of this difference is not clear, but it is very likely related to the diffusion of alkaline or alkaline earth ions (Na^+, Ca^{2+}, etc.) from the glass substrate, which slightly deactivate the catalysts [42]. Incorporation of Zr may favor this process, turning the doped coating more sensitive to the nature of the substrate. In this respect, the present results suggest that when silicon is used as support, and consequently, diffusion of Na^+ cannot occur, incorporation of Zr can improve the photoactivity of

the TiO_2 coating about 25%. In this case an increment can be related mainly to the higher specific surface, as suggested by the specific activities by surface area, but an influence of the new active surface sites in the oxide interface can be also envisaged [27]. In contrast with the samples prepared from microemulsions, the crystalline size of the particles contained in these coatings is lower and, accordingly, the specific surface area is larger [26,27]. This low crystallinity, along with the relatively high Zr content, could justify why the performance of the SS coating is similar to that of TiO_2, despite its high surface area and in contrast with previous reports on the beneficial effect of Zr-doping [24,27].

The *operando* FTIR study reveals that variations in coating composition lead to rather distinct concentration of adsorbed intermediates. Thus, the presence of Zr centers seems to favor the build-up of formates, while in the case of the TiO_2 coating only a small amount of aldehydes is present. These variations can be explained not only by differences in adsorption capacity caused by Zr incorporation, but also by changes in the rate of the different surface reactions. Thus, it is worth noting that although sample SS presents the highest acetone adsorption capacity, its photoactivity is the lowest. The simplified kinetic analysis shows that the rate for formate decomposition is remarkable lower on the SS coating than for Z/T and consequently a higher coverage is achieve on this sample. Considering the absence of these carboxylates on the TiO_2 film, it seems that these species are preferential adsorbed on either Zr cations or sites located in its close vicinity. Consequently, it can be hypothesized that on the Z/T coatings the patchy distribution of ZrO_2 leaves TiO_2 areas available for the formation of oxidant radicals. In contrast, due to the most homogenous distribution of the dopant in the SS coating, formation of active radicals like O^- may be hindered over the whole surface when the formate concentration is high. In any case, the present results indicate that not only the electronic properties of the film but also the surface characteristics of the semiconductor are crucial for photocatalysis. These two variables exert a paramount influence on the photocatalytic reaction rate of these different materials. Furthermore, variation of surface features has a different effect on each elemental process of the acetone degradation mechanism.

5. Conclusions

The results obtained in this study indicate that *operando* FTIR spectroscopy is a very powerful tool to study molecular details of photocatalytic reactions over semiconductors films. Furthermore, the use of thin films ensures a completed irradiation of the whole semiconductor, and consequently information about photochemical reactions can be obtained without the interference of dark processes. In absence of UV-light acetone adsorbs molecularly on the films composed of TiO_2, $Ti_{1-x}Zr_xO_2$ or mixtures of ZrO_2 and TiO_2. The higher absorption capacity corresponds to the $Ti_{1-x}Zr_xO_2$ coating, as expected due to its higher specific surface. However, the maximum photocatalytic rate for acetone degradation corresponds to the films formed by a binary mixture of TiO_2 and ZrO_2. The analysis of the surface species reveals notable differences on the type and concentration of adsorbed intermediates on the coatings studied. Thus, formate accumulates on both films containing Zr, but they are removed at a considerable lower rate on the $Ti_{1-x}Zr_xO_2$ coating, and this fact contributes to the reduced photoactivity of this sample. On the other hand, the better performance of the film containing both ZrO_2 and TiO_2 is due not only to efficiency on the oxidation of adsorbed acetone but also to the higher rate for the decomposition of formates. In the case of the TiO_2 film, formaldehyde is the only intermediate detected in a significant concentration. Langmuir–Hinshelwood kinetic equation reproduces reasonably the evolution of the gas phase acetone and it is also compatible with the observed evolution of adsorbed species as the proposed kinetic model indicates.

Acknowledgements

Financial support from different research projects from the Spanish Ministry of Science and Innovation (MICINN) is greatly appreciated. M.D.H. also thanks MICINN for the award of a postdoctoral grant. We fully appreciated the valuable suggestions and criticism of the reviewers.

References

[1] A. Fujishima, X.T. Zhang, Comptes Rendus Chim. 9 (5–6) (2006) 750.
[2] A.A. Adesina, Catal. Surv. Asia 8 (4) (2004) 265.
[3] A.V. Emeline, V.K. Ryabchuk, N. Serpone, J. Phys. Chem. B 109 (39) (2005) 18515.
[4] T.L. Thompson, J.T. Yates, Chem. Rev. 106 (10) (2006) 4428.
[5] M. Kaise, H. Nagai, K. Tokuhashi, S. Kondo, S. Nimura, O. Kikuchi, Langmuir 10 (1994) 1345.
[6] A.L. Attwood, J.L. Edwards, C.C. Rowlands, D.M. Murphy, J. Phys. Chem. A 107 (11) (2003) 1779.
[7] T. Van der Meulen, A. Mattson, L. Österlund, J. Catal. 251 (2007) 131.
[8] A. Mattsson, M. Leideborg, K. Larsson, G. Westin, L. Osterlund, J. Phys. Chem. B 110 (3) (2006) 1210.
[9] C. Hagglund, B. Kasemo, L. Osterlund, J. Phys. Chem. B 109 (21) (2005) 10886.
[10] S. Kataoka, E. Lee, M.I. Tejedor-Tejedor, M.A. Anderson, Appl. Catal. B 61 (1–2) (2005) 159.
[11] J.M. Coronado, S. Kataoka, I. Tejedor-Tejedor, M.A. Anderson, J. Catal. 219 (1) (2003) 219.
[12] M. El-Maazawi, A.N. Finken, A.B. Nair, V.H. Grassian, J. Catal. 191 (2000) 138.
[13] W.C. Wu, C.C. Chuang, J.L. Lin, J. Phys. Chem. B 104 (2000) 8719.
[14] W.Z. Xu, D. Raftery, J. Catal. 204 (1) (2001) 110.
[15] W. Xu, D. Raftery, J. Phys. Chem. B 105 (2001) 4343.
[16] M.A. Bañares, Catal. Today 100 (1–2) (2005) 71–77.
[17] P.Z. Araujo, C.B. Mendive, L.A.G. Rodenas, P.J. Morando, A.E. Regazzoni, M.A. Blesa, D. Bahnemann, Colloid Surf. A 265 (1–3) (2005).
[18] S. Kataoka, M.I. Tejedor-Tejedor, J.M. Coronado, M.A. Anderson, J. Photochem. Photobiol. A 163 (3) (2004) 323.
[19] F. Fresno, D. Tudela, J.M. Coronado, M. Fernández-García, A.B. Hungría, J. Soria, Phys. Chem. Chem. Phys. 8 (2006) 2421.
[20] J.F. Zhu, Z.G. Deng, F. Chen, J.L. Zhang, H.J. Chen, M. Anpo, J.Z. Huang, L.Z. Zhang, Appl. Catal. B 62 (3–4) (2006) 329–335.
[21] A. Fuerte, M.D. Hernández-Alonso, A.J. Maira, A. Martínez-Arias, M. Fernández-García, J.C. Conesa, J. Soria, G. Munuera, J. Catal. 212 (2002) 1.
[22] R. Asahi, T. Morikawa, T. Ohwaki, K. Aoki, Y.Y. Taga, Science 293 (2001) 269.
[23] T. Kawahara, Y. Konishi, H. Tada, N. Tohge, S. Ito, Langmuir 17 (2001) 7442.
[24] X. Fu, L.A. Clark, Q. Yang, M.A. Anderson, Environ. Sci. Technol. 30 (1996) 647–653.
[25] J.C. Yu, J. Lin, R.W.M. Kwok, J. Phys. Chem. B 102 (1998) 5094–5098.
[26] M.D. Hernández-Alonso, I. Tejedor-Tejedor, J.M. Coronado, J. Soria, M.A. Anderson, Thin Solid Films 502 (2006) 125–131.
[27] M.D. Hernández-Alonso, J.M. Coronado, B. Bachiller-Baeza, M. Fernández-García, J. Soria, Chem. Mater. 19 (2007) 4283–4291.
[28] C.H. Wu, C.T. Feng, Y.S. Lo, T.Y. Lin, J.G. Lo, Chemosphere 56 (1) (2004) 71–80.
[29] A. Díaz-Parralejo, R. Carusob, A.L. Ortiz, F. Guiberteau, Thin Solid Films 458 (2004) 92–97.
[30] L. Liang, Y. Sheng, Y. Xu, D. Wu, Y. Sun, Thin Solid Films 515 (2007) 7765–7771.
[31] C. Arrouvel, M. Digne, M. Breysse, H. Toulhoat, P. Raybaud, J. Catal. 222 (2004) 152–166.
[32] J. Raskó, T. Kecskés, J. Kiss, J. Catal. 226 (2004) 183–191.
[33] T. Berger, M. Sterrer, O. Diwald, E. Knozinger, D. Panayotov, T.L. Thompson, J. Phys. Chem. B 109 (2005) 6061.
[34] A.W. Li, H. Xing, C.L. Zhou, J. Shen, L.T. Zhang, W. Zheng, Y.S. Zhang, Mater. Lett. 59 (29–30) (2005) 3896–3899.
[35] M.A. Henderson, J. Phys. Chem. B 109 (2005) 12062–12070.
[36] X. Ye, D. Chen, J. Gossage, K. Li, J. Photochem. Photobiol. A 183 (2006) 35–40.
[37] D.S. Muggli, J.T. McCue, J.L. Falconer, J. Catal. 173 (1998) 470–483.
[38] L.F. Liao, W.C. Wu, C.Y. Chen, J.L. Lin, J. Phys. Chem. B 105 (2001) 7678.
[39] K. Demeestere, A. De Visscher, J. Dewulf, M. Van Leeuwen, H. Van Langenhove, Appl. Catal. B 54 (4) (2004) 261.
[40] J.M. Coronado, M.E. Zorn, I. Tejedor-Tejedor, M.A. Anderson, Appl. Catal. B 43 (2003) 329.
[41] A. Mills, R.H. Davies, D. Worsley, Chem. Soc. Rev. (1993) 417.
[42] J. Yu, X. Zhao, Mater. Res. Bull. 35 (2000) 1293.